CHEMISTRY OF MATERIALS
Article

Chem. Mater. **2009,** *21,* 5119–5124 5119
DOI:10.1021/cm9020113

Interplay between Order and Disorder in the High Performance of Amorphous Transparent Conducting Oxides

Aron Walsh,*[,†] Juarez L. F. Da Silva,[§] and Su-Huai Wei[‡]

[†]*University College London, Department of Chemistry, Materials Chemistry, 3rd Floor, Kathleen Lonsdale Building, London WC1E 6BT, U.K.,* [‡]*National Renewable Energy Laboratory, Golden, Colorado 80401, and* [§]*Instituto de Física de São Carlos, Universidade de São Paulo, Caixa Postal 369, São Carlos, 13560-970 SP, Brazil*

Received July 6, 2009. Revised Manuscript Received September 22, 2009

We demonstrate, using first-principles calculations, that the exceptional behavior of amorphous transparent conducting oxides formed from In, Zn, Ga, and Al cations arises from the preservation of local crystal order in the cation centered polyhedra, which is maintained due to the strong charge transfer to oxygen. While tails of localized states may be created above the valence band, the highly delocalized conduction band remains unperturbed, offering effective *n*-type conduction despite the existence of long-range structural disorder. This is in direct contrast to the paradigm set by amorphous covalent semiconductors.

Introduction

Amorphous transparent conducting oxides (aTCOs) are becoming the materials of choice for optoelectronic applications.[1−5] They exhibit excellent electronic transport properties in stark contrast to traditional amorphous covalent semiconductors, and yet, their underlying chemical and physical characteristics have yet to be fully understood and explored.

In amorphous systems, the underlying crystalline nature of a material is destroyed, and the language we generally use to describe complex phenomena ranging from crystal phase transitions to anisotropic optical diffraction is lost. For covalent semiconductors such as Si, amorphization is associated with a substantial deterioration in conductivity, relative to the crystalline phase. This is due to the formation of unpassivated dangling bonds, which introduce tail states inside the band gap and deteriorate electron transport.[6] It is therefore remarkable that aTCOs can exhibit superior properties relative to their crystalline counterparts. How does this peculiar behavior arise?

To begin with, TCOs are themselves an exclusive class of materials. Their combination of visible light transmission with high electronic conductivity makes them essential for window layers in photovoltaic devices and for application in thin-film transistors and UV optoelectronic devices.[7,8] The prototype TCOs are metal oxides formed from ns^0 post-transition metal cations, namely, ZnO, In_2O_3, and SnO_2.[9−12] These materials exhibit intrinsic *n*-type behavior, which is often assisted by oxygen deficiency or cation interstitials,[13] and can be further substitutionally doped to exhibit low resistivities comparable to metallic conductors, e.g. ZnO:Al, In_2O_3:Sn, and SnO_2:F.[9]

The ever increasing demand to decrease TCO cost and to improve their stability and performance has led to the investigation of complex ternary and quaternary oxide systems with novel cation combinations.[1−5,14−18] To supplement the list of basic elemental ingredients (Zn, In, Sn), the addition of Ga and Al can serve both to increase the optical band gaps for UV applications and

(1) Nomura, K.; Ohta, H.; Takagi, A.; Kamiya, T.; Hirano, M.; Hosono, H. *Nature* **2004**, *432*, 488.
(2) Sun, Y.; Rogers, J. *Adv. Mater.* **2007**, *19*, 1897.
(3) Lee, D.-H.; Chang, Y.-J.; Herman, G.; Chang, C.-H. *Adv. Mater.* **2008**, *19*, 843.
(4) Taylor, M. P.; Readey, D. W.; van Hest, M. F. A. M.; Teplin, C. W.; Alleman, J. L.; Dabney, M. S.; Gedvilas, L. M.; Keyes, B. M.; To, B.; Perkins, J. D.; Ginley, D. S. *Adv. Funct. Mater.* **2008**, *18*, 3169.
(5) Kumar, B.; Gong, H.; Akkipeddi, R. *J. Appl. Phys.* **2005**, *98*, 073703.
(6) Mott, N. F. *Conduction in non-crystalline materials*, 1st ed.; Oxford Science Publications: Oxford, 1987.
(7) Fortunato, E.; Ginley, D.; Hosono, H.; Paine, D. C. *MRS Bull.* **2007**, *32*, 242.
(8) Thomas, G. *Nature* **1997**, *389*, 907.
(9) Edwards, P. P.; Porch, A.; Jones, M. O.; Morgan, D. V.; Perks, R. M. *Dalton Trans.* **2004**, *15*, 2295.
(10) Hamberg, I.; Granqvist, C. G.; Berggren, K. F.; Sernelius, B. E.; Engstrom, L. *Phys. Rev. B* **1984**, *30*, 3240.
(11) Walsh, A.; Da Silva, J. L. F.; Wei, S.-H.; Körber, C.; Klein, A.; Piper, L. F. J.; DeMasi, A.; Smith, K. E.; Panaccione, G.; Torelli, P.; Payne, D. J.; Bourlange, A.; Egdell, R. G. *Phys. Rev. Lett.* **2008**, *100*, 167402.
(12) Bourlange, A.; Payne, D. J.; Egdell, R. G.; Foord, J. S.; Edwards, P. P.; Jones, M. O.; Schertel, A.; Dobson, P. J.; Hutchison, J. L. *Appl. Phys. Lett.* **2008**, *92*, 092117.
(13) Kim, Y.-S.; Park, C. H. *Phys. Rev. Lett.* **2009**, *102*, 086403.
(14) Minami, T.; Sonohara, H.; Kakumu, T.; Takata, S. *Jpn. J. Appl. Phys.* **1995**, *34*, L971.
(15) Taylor, M. P.; Readey, D. W.; Teplin, C. W.; van Hest, M. F. A. M.; Alleman, J. L.; Dabney, M. S.; Gedvilas, L. M.; Keyes, B. M.; To, B.; Perkins, J. D.; Ginley, D. S. *Meas. Sci. Technol.* **2005**, *16*, 90.
(16) Hiramatsu, H.; Seo, W.-S.; Koumoto, K. *Chem. Mater.* **1998**, *10*, 3033.
(17) Leenheer, A. J.; Perkins, J. D.; van Hest, M. F. A. M.; Berry, J. J.; O'Hayre, R. P.; Ginley, D. S. *Phys. Rev. B* **2008**, *77*, 115215.
(18) Moriga, T.; Okamoto, T.; Hiruta, K.; Fujiwara, A.; Nakabayashi, I. *J. Solid State Chem.* **2000**, *155*, 312.

Published on Web 10/15/2009

crystal stability for commercial deployment. The search for new TCOs with lower In concentration is an important and active area due to the increasing scarcity and cost of In metal. However, even from these five cation combinations alone, ten ternary and ten quaternary systems exist, in which the relative cation compositions can be varied (e.g., $A^{III}_{2n}B^{II}_{m}O_{3n+m}$). It is therefore imperative to obtain a deep understanding of the underlying composition−structure−performance relationship so that the optimum material compositions can be designed and synthesized. One prototype quaternary material that has emerged recently is $InGaZnO_4$ (IGZO), which contains In, Ga, and Zn in a 1:1:1 ratio, and has been the subject of detailed investigation.[19−23]

Due to the high energetic cost of forming crystalline multicomponent oxides, producing amorphous thin films by low temperature processing is becoming standard and is especially desirable for widespread commercial application and for producing contacts for flexible optoelectronic devices. In particular, amorphous oxide films are amenable to low cost growth techniques (e.g., sputter deposition), and they combine thermal and chemical stability with excellent conductivity. After preliminary work by Hosono et al. on amorphous Cd_2GeO_4, $AgSbO_3$, and Cd_2PbO_4,[24] the breakthrough in this field came from the report by Nomura et al.[1] that the electron mobility of amorphous IGZO thin films exceeded 10 $cm^2\ V^{-1}\ s^{-1}$, more than an order of magnitude greater than a-Si. They attributed this remarkable behavior to the isotropy of the conduction band network,[1] which in most *n*-type TCOs is predominately composed of cation s orbitals.[25,26] Following this report, IGZO has become the most widely studied amorphous TCO and is a strong candidate for the electron-injection-layer for solid-state lighting devices.[1,21,27] Replacement of In with Sn to form $(Sn,Ga,Zn)O_n$ amorphous oxides has been investigated;[28] however, $(Sn,Ga,Zn)O_n$ based compounds were found to offer much poorer performance compared to IGZO due to the presence of a significant amount of tail states that inhibit the conductivity,[28] which may be linked to the accessibility of both the upper (4^+)[29,30] and lower (2^+)[31,32] oxidation states of Sn and the associated ionic charge compensation of excess electron carriers.

Typically in amorphous semiconductors, structural defects formed where the normal coordination environments are lost, produce states in the band gap, which can substantially deteriorate the electrical properties.[6] For amorphous silicon, the tail states, caused by dangling bonds, can be passivated through hydrogenation. In contrast, sub-band gap defect states are apparently not an issue for carrier transport in most aTCOs,[26] and even if produced, they can be controlled via low temperature (300 °C) annealing.[28] Theoretical work on amorphous IGZO, simulated using classical molecular dynamics,[33] found short-range coordination environments in good agreement with the crystalline structure[19] and extended X-ray absorption fine structure (EXAFS) measurements of the amorphous system,[33] which suggests a different paradigm to covalent semiconductors. In this work, we contrast the crystalline and amorphous phases of a wider range of TCOs, $In_2O_3(ZnO)$ (IZO), IGZO, and $InAlZnO_4$ (IAZO), from a first-principles electronic-structure perspective and demonstrate what makes this class of amorphous materials unique: the preservation of local cation coordination environments, driven by strong metal to oxygen charge transfer, is combined with long-range structural disorder to provide a dispersive and delocalized conduction band *without* the influence of tail states.

Computational Methods

Total energy electronic structure and molecular dynamics calculations were performed using density functional theory[34,35] (DFT) as implemented in the Vienna Ab Initio Simulation Package.[36,37] The Zn, Ga, and In shallow-core d^{10} states were treated as valence within the all-electron projector augmented wave method[38] and a plane-wave basis set (500 eV cutoff). Exchange and correlation effects (E_{xc}) were treated by the generalized gradient approximation, through the Perdew−Burke−Ernzerhof (PBE) functional.[39]

It is well-known that standard local or semilocal DFT exchange-correlation functionals underestimate the band gaps of insulators and semiconductors due to the discontinuity in the energy derivative.[40,41] For more quantitative bandgap estimations, we adopted the hybrid Heyd−Scuseria−Ernzerhof (HSE06) approach,[42,43] in which 25% of exact Hartree−Fock nonlocal exchange replaces the short-range (SR) PBE functional. The partitioning of the SR and

(19) Orita, M.; Tanji, H.; Mizuno, M.; Adachi, H.; Tanaka, I. *Phys. Rev. B* **2000**, *61*, 1811.
(20) Lee, W.-J.; Choi, E.-A.; Bang, J.; Ryu, B.; Chang, K. J. *Appl. Phys. Lett*. **2008**, *93*, 111901.
(21) Nomura, K.; Ohta, H.; Ueda, K.; Kamiya, T.; Hirano, M.; Hosono, H. *Science* **2003**, *300*, 1269.
(22) Omura, H.; Kumomi, H.; Nomura, K.; Kamiya, T.; Hirano, M.; Hosono, H. *J. Appl. Phys.* **2009**, *105*, 093712.
(23) Da Silva, J. L. F.; Yan, Y.; Wei, S.-H. *Phys. Rev. Lett*. **2008**, *100*, 255501.
(24) Hosono, H.; Kikuchi, N.; Ueda, N.; Kawazoe, H. *J. Non-Cryst. Solids* **1996**, *198−200*, 165.
(25) Medvedeva, J. E. *Euro. Phys. Lett*. **2007**, *78*, 57004.
(26) Robertson, J. *Phys. Status Solidi B* **2008**, *245*, 1026.
(27) Nomura, K.; Kamiya, T.; Yanagi, H.; Ikenaga, E.; Yang, K.; Kobayashi, K.; Hirano, M.; Hosono, H. *Appl. Phys. Lett*. **2008**, *92*, 202117.
(28) Hosono, H.; Nomura, K.; Ogo, Y.; Uruga, T.; Kamiya, T. *J. Non-Cryst. Solids* **2008**, *354*, 2796.
(29) Freeman, C. M.; Catlow, C. R. A. *J. Solid State Chem*. **1990**, *85*, 65.
(30) Godinho, K. G.; Walsh, A.; Watson, G. W. *J. Phys. Chem. C* **2009**, *113*, 439.
(31) Togo, A.; Oba, F.; Tanaka, I.; Tatsumi, K. *Phys. Rev. B* **2006**, *74*, 195128.
(32) Walsh, A.; Watson, G. W. *Phys. Rev. B* **2004**, *70*, 235114.
(33) Nomura, K.; Kamiya, T.; Ohta, H.; Uruga, T.; Hirano, M.; Hosono, H. *Phys. Rev. B* **2007**, *75*, 035212.
(34) Kohn, W.; Sham, L. J. *Phys. Rev*. **1965**, *140*, A1133.
(35) Hohenberg, P.; Kohn, W. *Phys. Rev*. **1964**, *136*, B864.
(36) Kresse, G.; Furthmüller, J. *Phys. Rev. B* **1996**, *54*, 11169.
(37) Kresse, G.; Furthmüller, J. *Comput. Mater. Sci*. **1996**, *6*, 15.
(38) Kresse, G.; Joubert, D. *Phys. Rev. B* **1999**, *59*, 1758.
(39) Perdew, J. P.; Burke, K.; Ernzerhof, M. *Phys. Rev. Lett*. **1996**, *77*, 3865.
(40) Perdew, J. P.; Levy, M. *Phys. Rev. Lett*. **1983**, *51*, 1884.
(41) Sham, L. J.; Schlüter, M. *Phys. Rev. Lett*. **1983**, *51*, 1888.
(42) Heyd, J.; Scuseria, G. E.; Ernzerhof, M. *J. Chem. Phys*. **2003**, *118*, 8207.
(43) Paier, J.; Marsman, M.; Hummer, K.; Kresse, G.; Gerber, I. C.; Angyan, J. G. *J. Chem. Phys*. **2006**, *124*, 154709.

long-range (LR) potentials was determined by a screening of $\omega = 0.11$ bohr^{-1}, i.e.

$$E_{xc}^{HSE}(\omega) = E_x^{HSE,SR} + E_x^{PBE,LR} + E_c^{PBE} \quad (1)$$

where

$$E_x^{HSE,SR} = \frac{1}{4}E_x^{Fock} + \frac{3}{4}E_x^{PBE} \quad (2)$$

The HSE06 results were then used to augment the band gaps in the PBE-calculated density of states and optical absorption spectra due to high computational scaling of the hybrid functional with increasing number of atoms per unit cell for the large system sizes studied.

The layered modulated crystalline structures, containing 4 f. u. per cell, were taken from a recent first-principles structural study.[23] A k-point grid density of $4 \times 4 \times 2$ was employed for these systems, with a double density mesh ($8 \times 8 \times 4$) used for calculating the electronic density of states and optical properties. The single-particle optical absorption spectra were calculated within the transversal approximation:[44] the optical transition matrix elements $\langle\psi_i|\hat{P}|\psi_f\rangle$, between states i and f with the momentum operator $\hat{P}$, were used to construct the imaginary part of the dielectric function, with the Kramers−Kronig transformation employed to generate the real part, from which the optical absorption can be directly derived.[45]

The amorphous structures were generated using first-principles molecular dynamics (DFT−PBE), for cell sizes up to 448 atoms (64 f.u. per cell), with k-point sampling restricted to the Γ point only. The starting structures were cubic supercells based on the spinel or layered modulated ternary structures, which were heated to 2000 K within a Nosé canonical ensemble for 10 ps, using a time step of 2 fs, to remove structure memory effects. After equilibration at 2000 K, the temperature was lowered to 1000 K for 20 ps and then rapidly quenched to 0 K (100 K/ps). The qualitative results were found to be insensitive to both the starting structure and cell size; the final results presented were obtained using 224 atom (32 f.u.) cells.

It is well-established that the energy landscape for amorphous systems is highly complex[46] with an intractable number of competing local mimina. Through the quenching process, we are just sampling a small number of specific local structural minima; any extension beyond this approach will prove problematic due to the excessive computational demands.

Finally, the total energies and electronic properties were obtained by full relaxation of the volume and atomic positions of the supercell to minimize the quantum mechanical stresses and forces. The densities of states and optical absorption spectra for the aTCOs were obtained using a $3 \times 3 \times 3$ k-mesh integrated within the tetrahedron method with Blöchl corrections.[47] All structure and electron density visualization was performed using VESTA.[48]

Results

Structural Properties. The optimized structures of the crystalline and amorphous phases of IZO are shown in Figure 1. In the crystalline phase, the structure is defined by mixed InO and ZnO polyhedra (bipyramids and tetrahedra) sandwiched between octahedral InO_2 planes. For IGZO and IAZO, the layered InO_2 octahedra are maintained, with Al and Ga replacing the interlayer InO units.[23] Remarkably, in the amorphous phases, these local coordination motifs are also present.

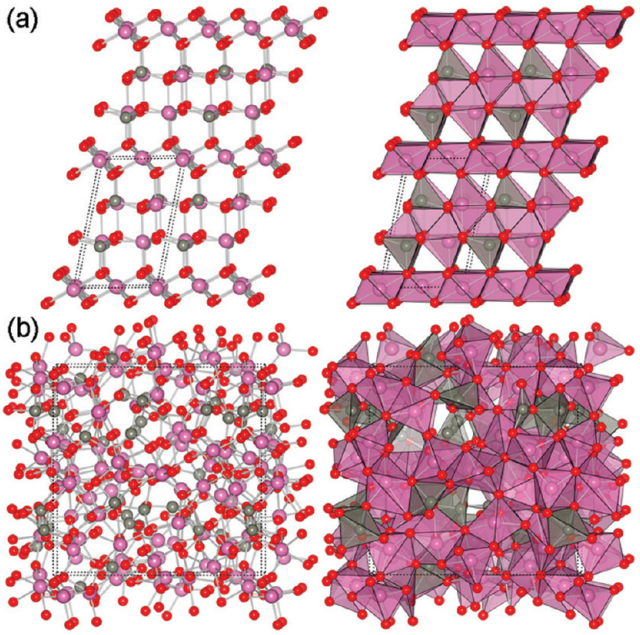

Figure 1. Structure representations of (a) crystalline and (b) amorphous $In_2O_3(ZnO)$ where the In atoms are colored pink, Zn gray, and O red. The cation coordination polyhedra are shown for the same structures on the right.

In order to directly compare the local order in both phases, we have calculated the effective coordination number[49,50] (ECN) and average pair correlation functions for both phases. The ECN is calculated by taking into account the individual metal−oxygen bond lengths (l_i) and their deviation with respect to the weighted average bond length, l_{av}, in the local polyhedra, i.e.

$$ECN = \sum_i \exp\left(1 - \left(\frac{l_i}{l_{av}}\right)^6\right) \quad (3)$$

where l_{av} is defined as

$$l_{av} = \frac{\sum_i l_i \exp\left(1 - \left(\frac{l_i}{l_{min}}\right)^6\right)}{\sum_i \exp\left(1 - \left(\frac{l_i}{l_{min}}\right)^6\right)} \quad (4)$$

with respect to the minimum bond length (l_{min}) in the polyhedra. This provides a more quantitative description of the classical coordination number and allows for a quick and robust comparison between coordination environments in different crystal structures. We found that the ECN average is 3.98 for Zn in the crystalline phase of

(44) Adolph, B.; Furthmüller, J.; Bechstedt, F. *Phys. Rev. B* **2001**, *63*, 125108.
(45) Segev, D.; Wei, S.-H. *Phys. Rev. B* **2005**, *71*, 125129.
(46) Middleton, T. F.; Wales, D. J. *Phys. Rev. B* **2001**, *64*, 024205.
(47) Blöchl, P. E.; Jepsen, O.; Andersen, O. K. *Phys. Rev. B* **1994**, *49*, 16223.
(48) Momma, K.; Izumi, F. *J. Appl. Crystallogr.* **2008**, *41*, 653.
(49) Hoppe, R.; Voigt, S.; Glaum, H.; Kissel, J.; Muller, H. P.; Bernet, K. *J. Less-Common Met.* **1989**, *156*, 105.
(50) Hoppe, R. *Angew Chem., Int. Ed. Engl.* **1970**, *9*, 25.

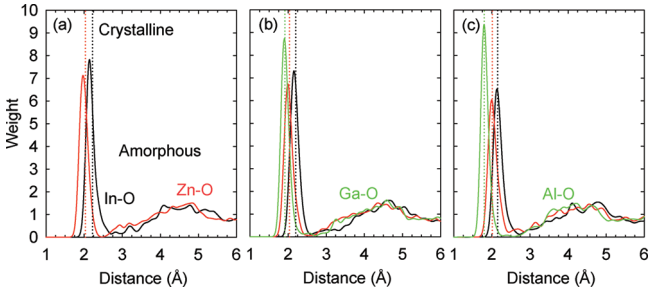

Figure 2. Calculated ion-averaged pair distribution functions for amorphous (a) $In_2O_3(ZnO)$, (b) $InGaZnO_4$, and (c) $InAlZnO_4$. The reference nearest-neighbor bond lengths in the corresponding crystalline phase are indicted by the dashed vertical lines. Outside the first coordination sphere (sharp peaks), no long-range ordering is observed.

Table 1. Calculated Equilibrium Volume per f.u. and Predicted HSE06 Band Gaps for the Amorphous Ternary and Quaternary Oxides, with the Corresponding Values for the Crystalline Phases Shown in Parentheses[a]

compound	volume (Å^3)	E_g (eV)	ΔE (meV)
$In_2O_3(ZnO)$	102.43 (94.96)	2.17 (2.56)	176
$InGaZnO_4$	94.90 (85.15)	2.24 (3.06)	187
$InAlZnO_4$	87.75 (81.69)	2.56 (3.61)	188

[a] ΔE, the formation energy per atom relative to the crystalline phase, is also shown.

IZO, close to the ideal wurtzite ZnO value of 4.00. In the amorphous phase, the value is marginally reduced and fluctuates between 3.5 and 4.0. Indium exhibits more flexibility in its coordination environment as demonstrated by bixbyite In_2O_3 itself, where the ECN is found to vary from 5.89 to 6.00 for the two crystallographically unique In sites. In IZO, the crystalline In ECN averages from 6.00 (4.66) for the octahedral (bipyramidal) atoms to a 4.2−5.8 range in the amorphous phase. The associated equilibrium polyhedra volumes[51] follow a similar trend. Furthermore, as shown from the ion-averaged pair correlation functions for IZO (Figure 2), the first coordination shell around In and Zn is well-defined with bond lengths only marginally contracted (less than 2%) from the crystalline phases. These local environments are in good agreement with recent EXAFS analysis for IGZO.[52] However, outside the first coordination shell, no ordering is ascertained. Similar results are obtained for IGZO and IAZO.

This analysis establishes the fact that the amorphous phases are defined by the random packing of cation centered polyhedra, i.e. the rigid anion sublattice present in the crystalline phases is eroded. While the manifestation of structural disorder is associated with a volume increase on the order of 7−12%, Table 1, the calculated ion-averaged partial charges derived from Bader analysis[53,54] flucuate within a small range (±0.05 electrons) confirming again that the local bonding preferences and charge neutrality are preserved. That is, even in the amorphous phase, the strong charge transfer between the metal cations and oxygen is preserved. While this is to be expected due to the large electronegativity of oxygen, it is in stark contrast to covalent semiconductors, where amorphization can be accurately represented as a series of local bond rearrangements that peturb the nearest neighbor enviornments.[55]

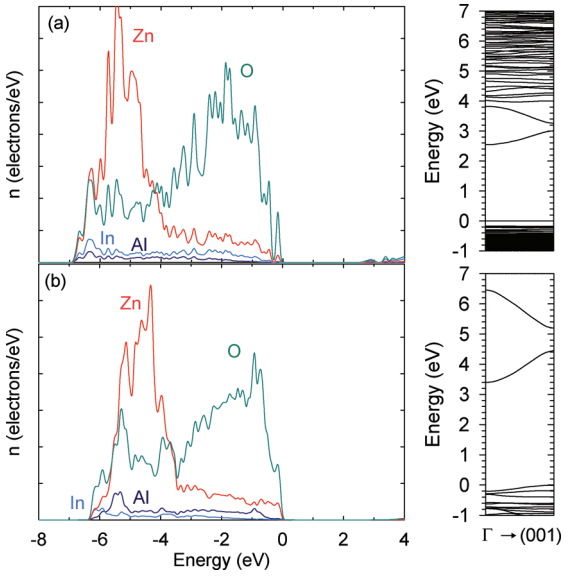

Figure 3. Partial electronic densities of states and electronic band dispersion in the (001) direction of (a) amorphous and (b) crystalline $InAlZnO_4$. The highest occupied state is set to 0 eV for each case.

The total energy difference between the crystalline and amorphous TCOs is on the order of 200 meV per f.u. in each system studied, Table 1, which is expected based on the increased strain due to the quasi-random packing of the cation centered polyhedra on amorphization. Despite their high energy, the aTCOs remain metastable experimentally at standard temperatures as they do not have sufficient energy to overcome the kinetic barriers for recrystallization.

Electronic Properties. The predicted band gap data, employing the hybrid HSE06 functional, are listed in Table 1. For the crystalline compounds, the band gaps follow the clear trend of the group 13 binary oxides, increasing from In to Ga to Al. For the amorphous compounds, the same band gap trend is observed, but the magnitudes are lower compared to the crystalline structures. To understand whether this arises from perturbation of the valence or conduction bands, we can examine the electronic density of states, Figure 3. The valence band is composed of mostly O 2p states with some Zn 3d contributions. The features are typical of the crystalline materials.[20,56] The conduction band density of states is slow to rise, and from examination of the electronic band dispersion, this can be confirmed as a highly dispersive band characteristic of predominately ns^0 cation semiconductors. The dispersion is diminished, but still substantial for the aTCOs.

The main difference in the amorphous phase comes from the series of bands situated at the top of the valence

(51) Swanson, D. K.; Peterson, R. C. *Can. Mineralog.* **1980**, *18*, 153.
(52) Cho, D.-Y.; Song, J.; Na, K. D.; Hwang, C. S.; Kim, J.-Y.; Jeong, J. H.; Jeong, J. K.; Mo, Y.-G. *Appl. Phys. Lett.* **2009**, *94*, 112112.
(53) Bader, R. *Atoms in Molecules: A Quantum Theory*; Oxford University Press: New York, 1990.
(54) Sanville, E.; Kenny, S. D.; Smith, R.; Henkelman, G. *J. Comput. Chem.* **2007**, *28*, 899.
(55) Wooten, F.; Winer, K.; Weaire, D. *Phys. Rev. Lett.* **1985**, *54*, 1392.
(56) Walsh, A.; Da Silva, J. L. F.; Yan, Y.; Al-Jassim, M. M.; Wei, S.-H. *Phys. Rev. B* **2009**, *79*, 073105.

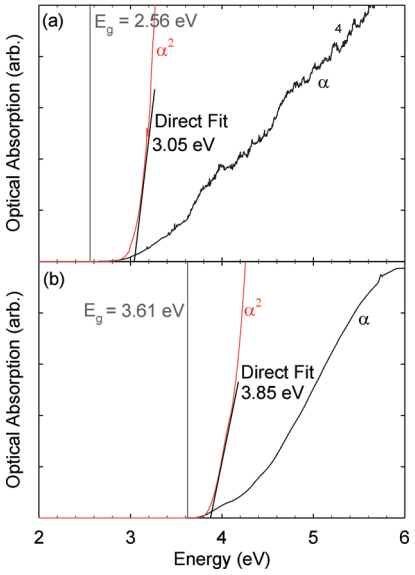

Figure 4. Simulated optical absorption spectra resulting from direct single particle transitions in (a) amorphous and (b) crystalline $InAlZnO_4$. The black lines represent the as calculated spectra, whereas the red lines are the square of the spectra, which is linearly extrapolated to zero absorption to estimate an effective direct optical band gap.

band. This contribution of the valence band to the sub band gap states has been confirmed in recent hard X-ray photoemission measurements[27] and is consistent with the band gap decrease observed for aTCOs.[5] As these states are highly localized in the Zn-rich regions, their contribution to visible range optical absorption (α) is small because the CBM is more localized on the group 13 cation side. On the basis of direct transitions and the Tauc relation ($E_g^{opt} \propto \alpha^2$),[57] which is regularly used in experimental assessment of the optical band gap,[5,17] we estimate a 0.5 eV difference between the fundamental and optical band gaps in the amorphous phase, while for the crystalline material this difference is 0.25 eV due to weak band-edge transitions typical of In containing oxides,[11] Figure 4.

It is also worth noting that when rapid quenching is employed (>200 K ps^{-1}), the formation of peroxide anions is observed, $(O_2^{2-})_O^x$ in Kröger−Vink notation. These act as a potential source of intrinsic carriers, effectively creating an oxygen vacancy in a nominally stoichiometric system, i.e. they may be viewed as an uncompensated anion Frenkel pair:

$$2O_O \rightleftharpoons O_O + O_i'' + V_O^{\cdot\cdot} \rightleftharpoons (O_2)_O^x + V_O^{\cdot\cdot} + 2e' \qquad (5)$$

Peroxide anions have been reported in other metal oxide systems, such as defective SnO_2[30] and ZnO,[58] but their prediction may be related to the typical overbinding of the O_2 molecule by standard DFT functionals such as PBE.[39] Their experimental presence may be revealed[59] by a characteristic Raman absorption band around 730 cm^{-1}.

(57) Wood, D. L.; Tauc, J. *Phys. Rev. B* **1972**, *5*, 3144.
(58) Sokol, A. A.; French, S. A.; Bromley, S. T.; Catlow, C. R. A.; van Dam, H. J. J.; Sherwood, P. *Faraday Discuss.* **2007**, *134*, 267.
(59) Gao, Z.-X.; Kim, H.-S.; Sun, Q.; Stair, P. C.; Sachtler, W. M. H. *J. Phys. Chem. B* **2001**, *105*, 6186.

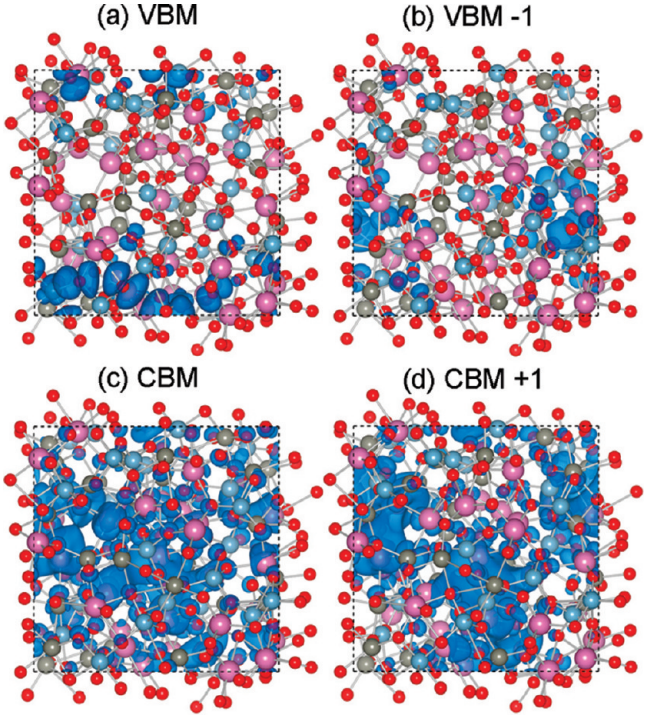

Figure 5. Band decomposed charge density isosurfaces of the band edge states in $InAlZnO_4$, where VBM represents the valence band maximum (highest occupied state) and CBM represents the conduction band minimum (lowest unoccupied state). CBM + 1 and VBM − 1 represent the electronic states above and below the band edges, which may become active in electron or hole doping, respectively.

The amorphous electronic density of states has important consequences. Most significantly for *n*-type conductivity, the conduction band remains highly delocalized, which can be understood from the overlap between the disperse cation s orbitals and the isotropic nature of the cation s−O 2s bonding.[1,25,26] As shown in the conduction band electron density, Figure 5c and d, the overlap is largely unaffected by the long-range structural disorder. As expected from their larger In−O bond lengths, In makes the largest contribution to the antibonding conduction band minimum. For IZO, $^2/_3$ of the cations are In, while for IGZO and IAZO, only $^1/_3$ In are present. Even for the lower concentration, the In−O polyhedra form a combination of edge and corner sharing networks ensuring that the conduction band is appropriately spread over the entire cell. This also gives a hint at why the amorphous low indium concentration TCOs can give even superior performance: in the crystalline compounds, the In−O networks become confined to two-dimensional planes separated by the Zn and group 13 cations, while in the amorphous compounds, the indiums become more homogeneously distributed and hence offer improved isotropic electron transport.

The upper valence band, however, follows a different fate. The cation d−O 2p derived bonding, which contributes to the top of the valence band, is highly anisotropic and depends on the structural alignment between neighboring polyhedra. This is clearly observed in the valence band electron density (Figure 5a and b), where states of similar atomic character are

separated in real space, confined to different regions of the unit cell, as well as energetically in the electronic band structure.

From our analysis, it is clear that while aTCOs exhibit excellent *n*-type conductivity, the *p*-type behavior should be poor due to the localization of the upper valence band states. The majority of *p*-type TCOs such as $CuAlO_2$ and $SrCu_2O_2$ are derived from Cu_2O,[60,61] where electron deficiency (hole formation) is facilitated by Cu oxidation.[62] In this case, polaron mobility will be inhibited by the structural disorder on amorphization. The absence of a *p*-type response has been noted experimentally,[27] and it is difficult to envisage an approach which would overcome this limitation.

Summary

In conclusion, while translational symmetry is lost on amorphization of metal oxides formed from In, Zn, Al, and Ga cations, the local metal−oxygen coordination motifs are well preserved. It is only the long-range packing of these polyhedra that is absent. This distinguishes the aTCOs from covalent amorphous semiconductors; the first coordination shell of the metal cations will always be saturated in order to facilitate complete charge transfer and satisfy the high electronegativity of the oxygen anions. This phenomenon preserves the preferred charge states of the component ions, ensuring that the main features of valence band and, most importantly, the cation s derived conduction band are maintained. The sub-band gap states produced on amorphization arise only from the valence band, where the covalent bonding (orbital interactions) is more isotropic. The absence of gap states near the conduction band explains why aTCOs behave as excellent *n*-type conductors and also the lack of *p*-type performance.

Acknowledgment. We would like to thank Yanfa Yan and Yong-Hyun Kim for useful discussions. The work is funded by the U.S. Department of Energy (DOE), under Contract No. DE-AC36-08GO28308. Computing resources of the National Energy Research Scientific Computing Center were employed, which is supported by DOE under Contract No. DE-AC02-05CH11231.

(60) Nie, X.; Wei, S.-H.; Zhang, S. B. *Phys. Rev. Lett.* **2002**, *88*, 066405.
(61) Nie, X.; Wei, S.-H.; Zhang, S. B. *Phys. Rev. B* **2002**, *65*, 075111.
(62) Scanlon, D. O.; Morgan, B. J.; Watson, G. W.; Walsh, A. *Phys. Rev. Lett.* **2009**, *103*, 096405.